AD-A086 540 LASER ANALYTICS INC BEDFORD MA F/G 17/5
MODEL LS-2X LASER SOURCE DETECTOR TEST SYSTEM.(U)
MAY 80 DAAB07-78-C-2465
UNCLASSIFIED NL

END
DATE FILMED
8-80
DTIC

LEVEL II

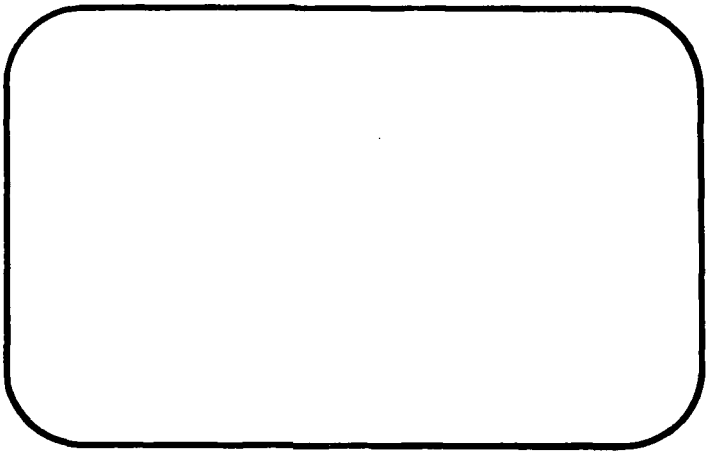

LASER ANALYTICS, INC.

(11) May 20

(9) Final rept.

FINAL REPORT

(6) MODEL LS-2X

LASER SOURCE DETECTOR

TEST SYSTEM

(12) 27

MAY 1980

(15)

Contract No. DAAB07-78-C-2465

Submitted to:

Commander, U.S. Army
CERCOM
Fort Monmouth, N. J. 07703

by

Laser Analytics, Inc.
25 Wiggins Ave.,
Bedford, Mass. 01730

TABLE OF CONTENTS

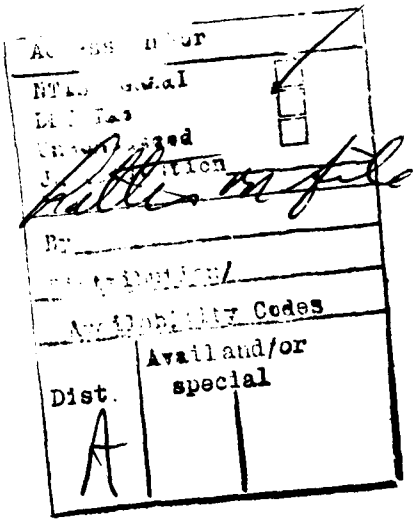

LIST OF ILLUSTRATIONS

LIST OF TABLES

1.0 INTRODUCTION

Proper characterization of infrared photodiodes requires a series of optical tests that include blackbody response, spatial uniformity, pulse response, and wavelength sensitivity measurements. The results of these optical tests will depend upon many fundamental properties of the detector crystal, namely absorption depth of the radiation, bulk lifetimes of injected carriers, surface recombination effects, carrier drift and diffusion effects, trapping effects and other mechanisms. Some of these effects are not clearly understood but may play important roles in such applications as high speed pulse detectors, laser heterodyne receivers, or large area high resolution detector arrays. Spears[1] has shown that proper spatial and temporal characterization of HgCdTe CO_2 laser heterodyne receivers must be done at the operating frequencies.

A realistic characterization of the pulse response of an infrared detector must be made at the operating wavelength, generally that of peak detector response. Certain fixed frequency gas lasers such as CO_2, CO, or HF can provide sufficient power and speed for detector characterization but they have limited wavelength coverage and are often cumbersome to use. On the other hand, Pb-salt tunable diode lasers can provide more than 100 μW of power emitted from nearly a point source, subnanosecond risetime pulses and wavelength selectability between 2.8 and 30 μm. These characteristics make diode lasers an ideal source for pulse and spatial response measurements of infrared detectors.

We have designed and tested an instrument that is capable of recording spatial sensitivity maps of detector elements, their temporal response function to nanosecond pulses, and potentially spatial maps of the temporal response. Large area arrays can also be uniformily illuminated with monochromatic radiation.

2.0 INSTRUMENT DESIGN

The emission characteristics of diode lasers are qualitatively that of a laser operating in high order transverse modes with several longitudinal modes. Since the junction region of the diode is small, the laser typically radiates into a diffration limited f/1 cone. Often, however, the output beams of individual lasers contain "hot" spots or high f-number lobes much more intense than the surrounding radiation. For the purposes outlined above, it is necessary to provide an expanded beam of uniform intensity (±10%) over a 10 mm disc to test large arrays and a focused spot of less than 100 μm diameter at λ = 5 μm to resolve the spatial profiles of small detector elements. It is therefore necessary to integrate or spatially filter the individual laser beams to achieve uniform and predictable results. We chose the spatial filter technique over that of integrating spheres, which has been investigated by Venkatesh and Mantz[2].

The optical layout of the instrument, hereafter called the Detector Test System or LS-2X, is shown in Figures 1-3. The basic system shown in Figure 1 consists of a tunable diode laser mounted in a stabalized closed cycle helium refrigerator, an initial ZnS, f/1 collimating lens, L, and plane mirror, M_1, mounted on a compound x-y-z stage, another plane mirror, M_2, and an off axis f/4 parabola, M_3, that focuses the radiation on a pinhole. The diverging radiation from the pinhole can be used to flood large area arrays as shown in Figure 1, collimated with an f/3.4 off axis parabola, M_5, as shown in Figure 2, or refocused for spatial mapping purposes with a second f/3.4 parabola, M_8, shown in Figure 3. The subplates containing mirror pairs, M_4 - M_6 and M_7 - M_9 are kinematically mounted, hence replaceable without loss of alignment.

The detector is mounted on a compound manually operated x-y-z stage. The detector element is typically located 140mm from the pinhole for all tests. Attached to two axes of the x-y-z stage are position transducers, linear variable differential transformers, which are used in conjunction with the manual drives of the x-y-z stage to produce raster scans on an analog x-y recorder.

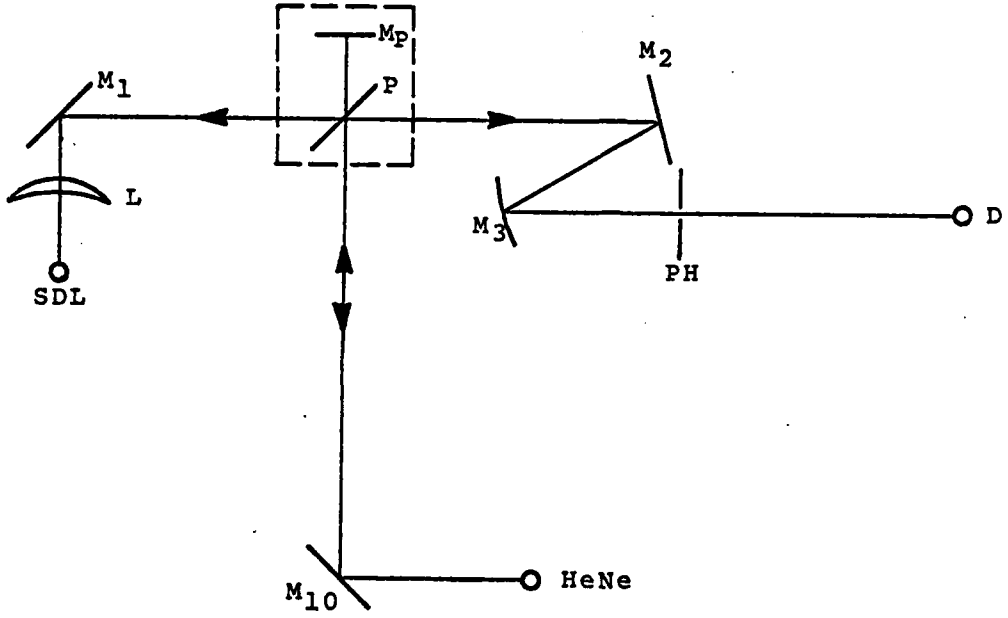

FIGURE 1

Fig. 1 Optical layout for far field measurements. M_1, M_2, M_{10}, and M_p are plane mirrors. L_3 is an f/1 lens, P is the pellicle, M_3 is an off axis parabola, and PH is the pinhole. The sources are the tunable diode laser, SDL, and the helium neon laser HeNe. D is the detector. The pellicle subassembly, P and M_p is in place. The arrows indicate the direction of the HeNe laser beam.

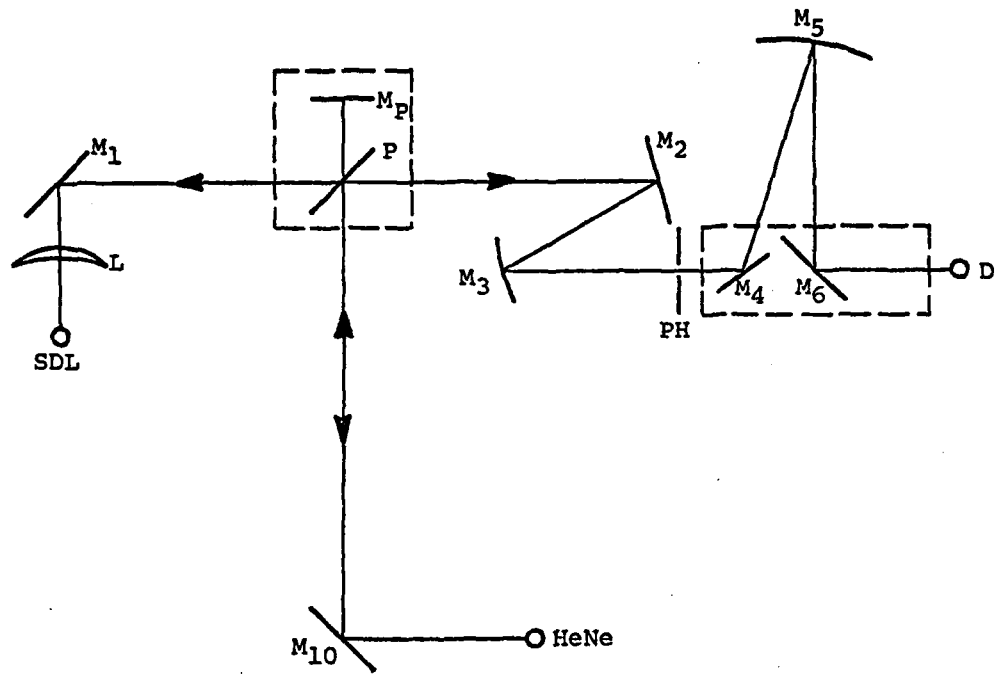

FIGURE 2

Fig. 2 Optical layout for collimated illumination of the detector, D,. M_4 and M_6 are plane mirrors on a kinematically mounted subplate; M_5 is an off axis parabola.

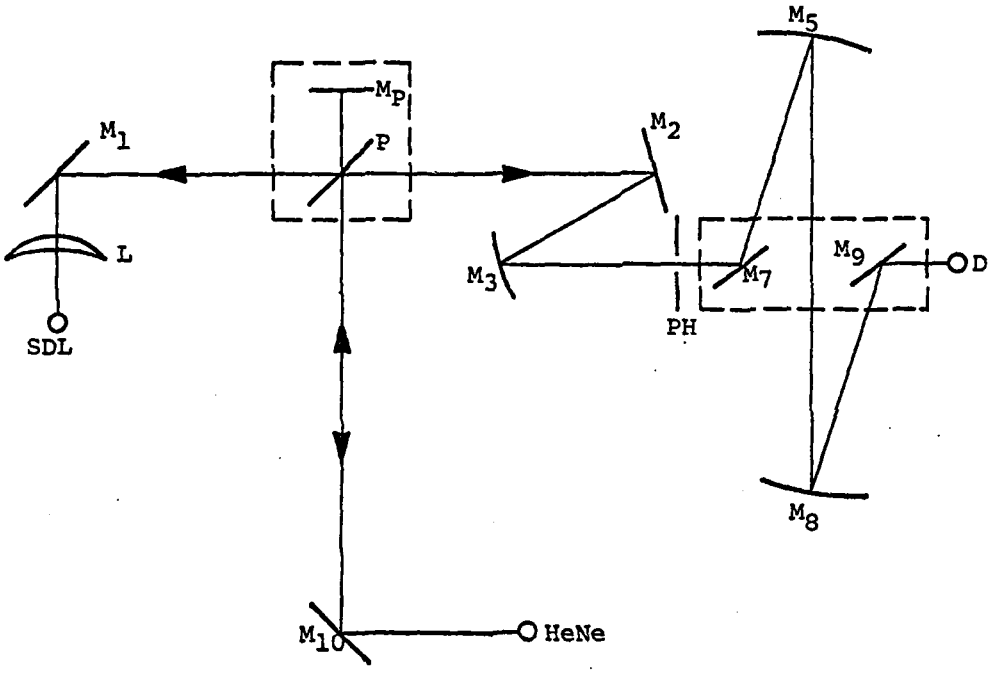

FIGURE 3

Fig. 3 Optical layout for focused spot illimination of the detector. Plane mirrors M_7 and M_9 are on a subplate. Mirror M_8 is an off axis parabola identical to mirror M_5.

A .6328 μm helium - neon laser is included in the LS-2X for alignment purposes. The He-Ne laser is permanently mounted and is optically inserted into the infrared beam via a pellicle beamsplitter, P, and a plane return mirror, M_P. This facilitates alignment of diode lasers, detectors, and pinholes.

A block diagram of the electronic components used in the LS-2X is shown in Figure 4. The CTS, Cryogenic Temperature Stabilizer provides precise (± 1 mK) temperature stability from 11K to over 100K while the LCM, Laser Control Module, supplies the d.c. current for the laser. Modulation of the optical signal is accomplished by chopping the d.c. current to the laser. The LCM has an internal chop mode with a frequency range of 500 Hz to 10 KHz. The LCP, Laser Current Pulser, is capable of delivering 10 ns and 100 ns wide pulses with risetimes less than 1 ns.

3.0 INSTRUMENT PERFORMANCE

3.1 Beam Uniformity

Fraunhofer diffraction at a circular aperature is a well known phenomenon. The intensity distribution[3] of the diffraction pattern first derived by Airy is given by[2]

$$I = I_o \left[\frac{2J_1(z)}{z} \right]^2 \quad (1)$$

where $z = ka \sin \alpha$ (2)

and $k = 2\pi/\lambda$, λ is the wavelength, a is the aperature radius, α is the diffraction half angle, J_1 is the first order Bessel Function, and I_o is the proportionately constant. The first order minimum occurs at

$$a \sin \alpha_1 = .61 \lambda. \quad (3)$$

For a pinhole radius $a = \lambda$, α_1 is 37.6°; hence, at 140 mm from the pinhole, the Airy disc has a radius of 108 mm. If the intensity at the center of the diffraction pattern is unity, then by Eq. (1), the intensity 5 mm from the optical axis should be 0.988.

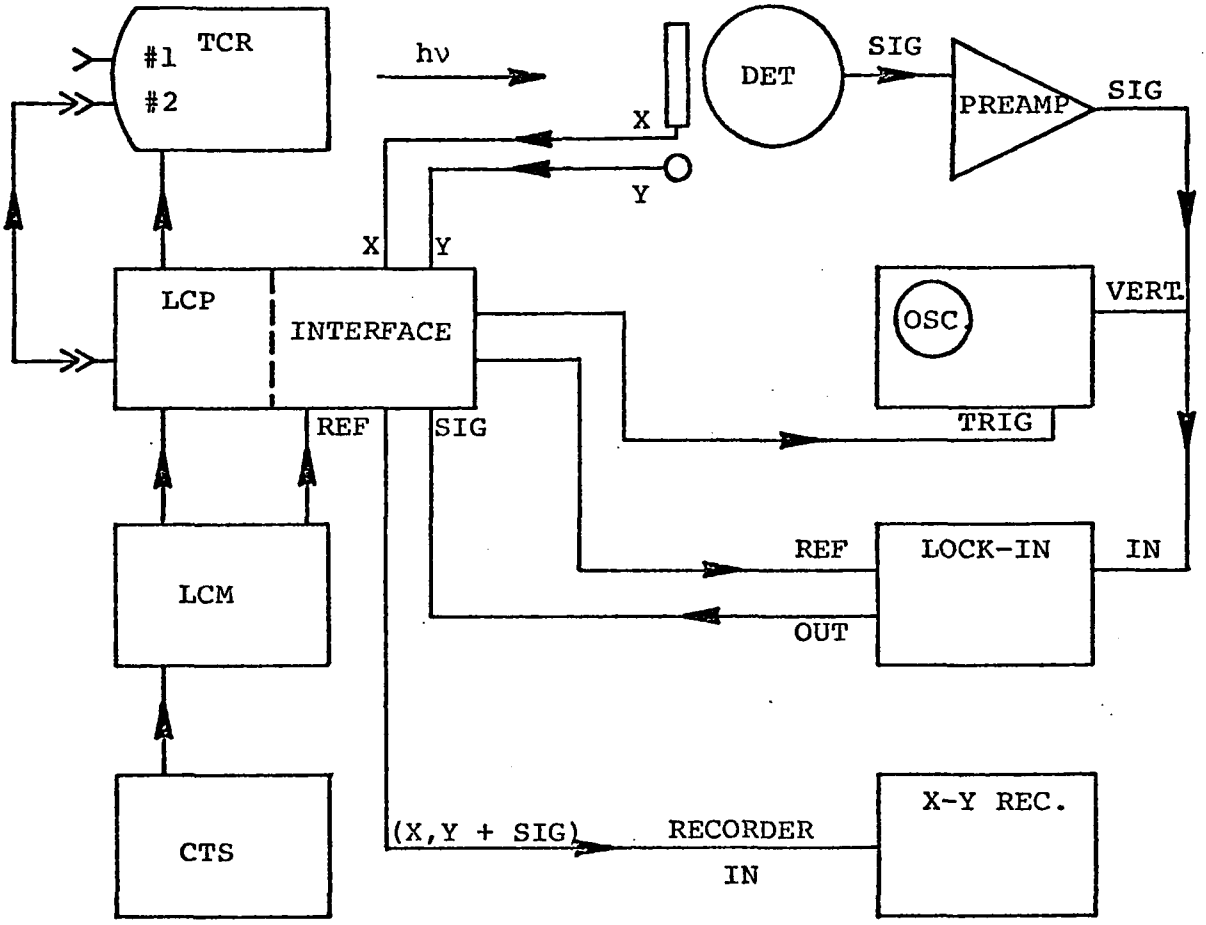

Fig. 4 Electrical Interconnections and flow diagram.

If the pinhole radius is 2.5λ, the first order minimum occurs at $\alpha_1 = 14.1°$ or an Airy disc radius of 35.2 mm at 140 mm. The minimum intensity within the central 10 mm diameter disc is 92.4% of the maximum intensity.

In practice, the far field beam uniformity did not coincide with the above figures. Tables I and II are typical digital raster scans of far field diffraction patterns. Both sets of data were recorded with the same 1 mm diameter InSb detector located 140 mm from the pinhole which was illuminated by a $\lambda = 5.03$ μm laser. The pinhole diameters were 11 μm and 25 μm respectively. The entire sampled area is 12.7 mm x 12.7 mm with .64 mm between samples. The demonstrated spatial uniformity within a 10 mm diameter disc is ± 5% and ± 5.5% respectively. Similar data, summarized in Table III, were recorded at 10.8 μm and 12.3 μm using a HgCdTe photoconductive detector with peak sensitivity near 16.3 μm. The element size was 1 mm square. The theoretical values of I_{min}/I_{max} were calculated from Eq. (1); the experimental values are for a 10 mm diameter disc at 140 mm from the pinhole. The power densities reported were calculated from the measured signal strength, the blackbody detector responsivity, and the preamplifier gain and hence are only approximate quantities. A power level of 10^{-10} W at the detector corresponds to a radiance of 5 $mW/mm^2 \cdot Sr$.

It is apparent that the experimental ratios of I_{min} to I_{max} in Table III do not agree with theory. This may be due to a number of reasons, namely convergent illumination of the pinhole, off axis illumination of the pinhole, or irregular pinhole shape. Nevertheless, all test scans were within the required uniformity specifications of ± 10% or $I_{min}/I_{max} = 0.80$.

3.2 Focused Spot Size

Spatial sensitivity mapping can be performed with the focused spot optical configuration in Figure 3. Theoretically, the electric field distribution of an aberation free image for a

coherently illuminated pinhole is given by the convolution of the pinhole transmission function with the diffraction pattern of the imaging optics, in this case mirrors M_5 and M_8. The electric field distribution function, E, is thus given by the two dimensional convolution integral[4,5]

$$E(r/f) = E_o \int_o^{2\pi} \int_o^a \frac{2J_1\,[kd\,(r-r')/f]}{kd\,(r-r')/f}\, r'\, dr'\, d\theta' \quad (4)$$

where E_o is a proportionately constant, d is the radius of the limiting aperature, f is the focal length of the mirrors, and r and (r',θ') are coordinate parameters, and $k = 2\pi/\lambda$. The intensity distribution is given by E^2.

Numerical evaluation of this integral would require significant computer time. For an infinitely small pinhole the results will be given by Eq. (1) which yields the minimum Airy disk diameter, b_{min}, of

$$b_{min} = 2.44\ \lambda\ (f/No). \quad (5)$$

For finite pinholes, the image diameter may be approximated by

$$b \sim (4a^2 + b_{min}^2)^{1/2} \quad (6)$$

where a is the radius of the pinhole.

No direct measurements of the spot size were made, but the approximate diameter can be inferred from the spatial resolution achieved in raster scans of detector elements. Figure 5 is a typical map of the 1 mm square HgCdTe photoconductive detector used above. This scan was recorded at $\lambda = 12.5$ μm with a 25 μm diameter pinhole. Figures 6 and 7 are raster scans of two different HgCdTe detectors which peak near 11 μm. These scans were made at $\lambda = 11.1$ μm with the same 25 μm diameter pinhole. The approximate theoretical Airy disc diameters from Eq. (6) for these two wavelengths are 107 μm and 95 μm respectively. The spatial resolution demonstrated by the sharpness or acutance at the edge of the detector elements indicate a spot sign of about 10% of the detector width or 100 μm which implies the system is diffraction limited and not aberation limited.

TABLE I

A far field intensity pattern measured at 140mm from a 11 μm diameter pinhole illuminated by λ = 5 μm radiation. Total area covered is 12.7 mm x 12.7 mm in .64 mm increments using a 1 mm diameter detector. The enclosed area represents a 10 mm diameter disk.

56	56	56	57	57	57	56	56	56	56	55	56	55	54	55	54	55	54	55	55
57	56	57	57	57	57	57	57	57	56	56	56	56	55	55	55	54	55	55	55
55	57	57	57	58	57	57	57	58	57	57	56	55	55	55	54	54	53	54	53
56	57	58	58	57	57	57	57	57	56	57	56	55	55	54	54	53	54	53	54
57	58	58	57	57	57	57	58	57	57	56	56	56	55	54	53	54	53	54	54
58	58	58	57	58	58	58	58	56	57	56	56	55	54	54	54	54	54	54	54
57	57	58	58	58	57	57	57	57	56	56	56	55	55	54	54	54	54	54	53
56	56	56	57	56	56	56	57	57	56	56	57	56	55	54	54	54	54	53	54
56	57	56	56	56	55	56	57	57	57	57	56	55	55	54	54	54	54	54	54
57	57	56	56	56	57	57	57	57	56	55	55	56	55	54	55	54	55	54	55
58	58	59	58	58	59	58	58	58	58	58	57	57	57	57	56	56	56	56	56
58	58	58	58	59	59	58	59	58	58	59	58	58	57	57	56	56	56	56	56
59	59	59	59	59	60	59	59	59	60	59	58	58	57	57	57	58	56	56	57
58	58	59	59	59	59	59	59	59	59	59	58	58	58	57	56	56	57	56	56
58	58	58	59	60	59	59	59	59	59	58	58	58	58	57	56	56	56	56	56
57	58	58	58	59	58	59	60	59	59	59	58	58	57	56	56	57	56	56	56
57	58	57	57	58	59	59	59	59	60	59	59	58	57	57	56	57	57	56	55
57	57	58	58	58	58	59	58	58	57	57	57	57	56	56	55	55	55	55	56
56	57	58	58	58	58	58	59	58	57	57	57	57	56	56	56	56	55	56	56
55	57	57	58	57	58	58	58	58	58	57	57	57	56	56	56	56	56	55	55

TABLE II

A far field intensity pattern recorded under the same experimental conditions as Table I except using a pinhole diameter of 25 μm.

87	88	89	90	91	91	93	93	93	93	94	93	92	91	90	89	90	90	90	90
88	89	91	92	93	94	94	94	95	94	94	94	93	94	92	92	91	91	91	91
89	91	93	93	94	95	96	97	97	96	95	95	95	94	93	92	92	92	93	92
90	92	94	95	96	98	98	98	99	98	97	96	96	95	94	93	94	93	93	93
92	94	95	96	98	99	99	99	100	99	99	98	96	96	94	93	93	93	94	94
91	95	97	98	99	99	100	101	101	101	100	99	97	96	95	94	94	95	95	94
93	95	97	98	99	100	101	100	101	100	100	99	97	96	96	94	94	95	94	94
95	97	97	99	98	101	101	102	101	101	101	99	99	97	96	95	95	95	95	95
95	98	99	101	101	102	102	102	102	102	102	100	100	98	97	96	96	96	96	96
95	97	99	100	102	102	102	102	102	102	102	102	100	99	97	95	95	95	96	96
95	98	98	100	101	102	102	102	102	102	102	101	99	98	96	95	95	95	95	95
95	97	99	98	100	101	101	102	102	102	102	101	99	97	95	94	94	94	94	95
95	95	98	99	100	101	101	101	101	101	100	99	98	97	94	94	94	94	94	93
93	95	97	98	100	100	100	100	100	99	98	98	96	95	93	92	92	92	93	92
92	93	95	97	97	98	99	98	98	98	96	96	94	94	92	91	91	91	91	90
91	92	94	95	97	97	97	98	97	96	96	94	92	92	91	89	89	89	89	89
89	91	92	92	94	95	95	95	95	94	94	93	92	91	89	88	89	88	87	88
88	89	90	91	93	93	93	94	93	93	92	91	90	89	88	86	86	86	86	86
85	86	88	90	90	90	92	91	91	90	89	88	88	86	85	84	84	84	84	84
82	83	86	86	87	88	88	89	88	88	87	87	86	85	83	82	81	82	82	82

TABLE III

UNIFORMITY OF FAR FIELD DIFFRACTION PATTERN

$\lambda/\mu m$	$2a/\mu m$	I_{min}/I_{max} Theor.	I_{min}/I_{max} Exp.	Power/$(10^{-10}W)$ Approx.
5.03	11	0.985	0.90	100
5.03	25	0.931	0.89	4200
10.8	25	0.983	0.85	120
10.8	50	0.938	0.89	580
12.3	25	0.988	0.87	6.6
12.3	50	0.949	0.84	39

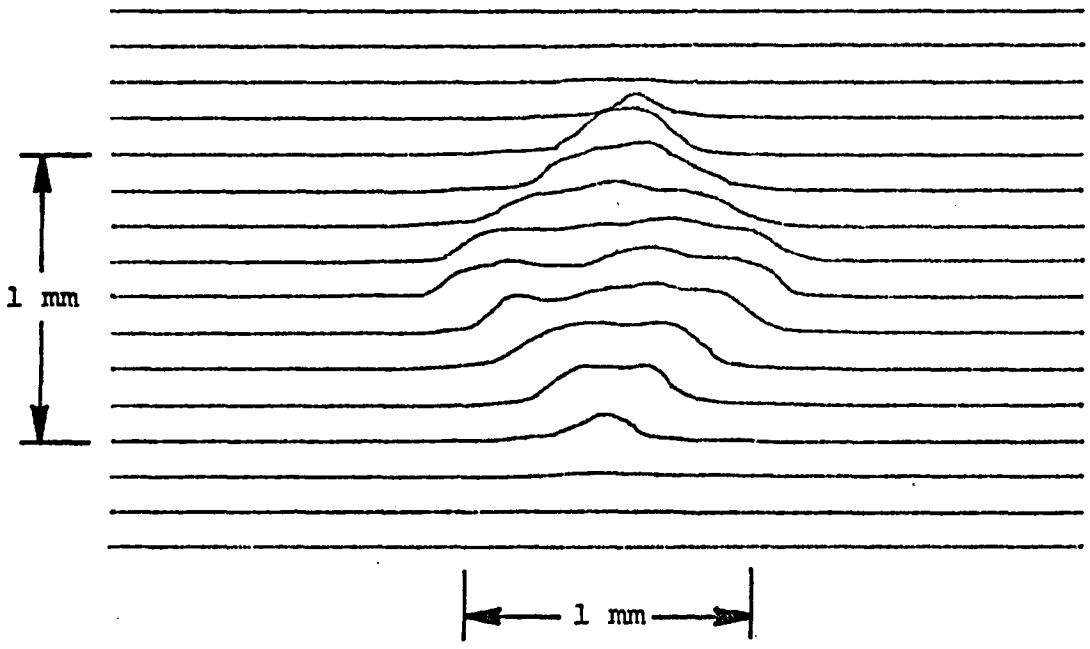

Fig. 5 A Raster scan of a 16.3 μm peak, photoconductive HgCdTe detector. The test wavelength is 12.5 μm, the pinhole size is 25 μm, and the detector element is 1 mm x 1 mm.

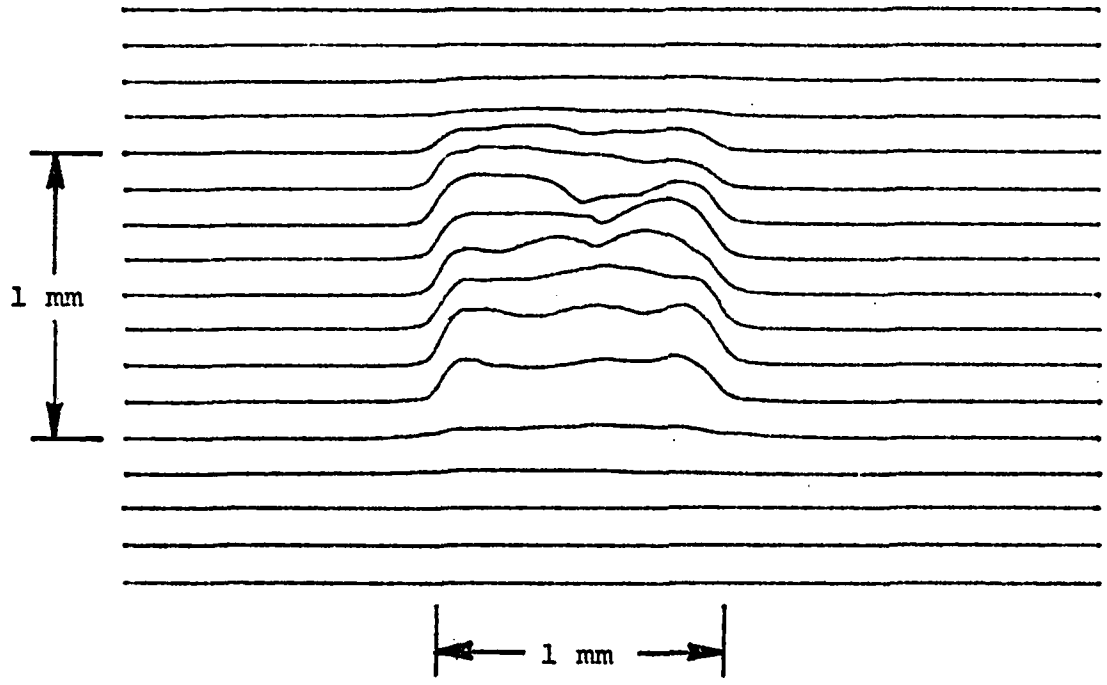

Fig. 6 Raster scan of a 1 mm square photoconductive HgCdTe detector. The test wavelength is 11.1 μm; the detector's sensitivity peaks near 11 μm.

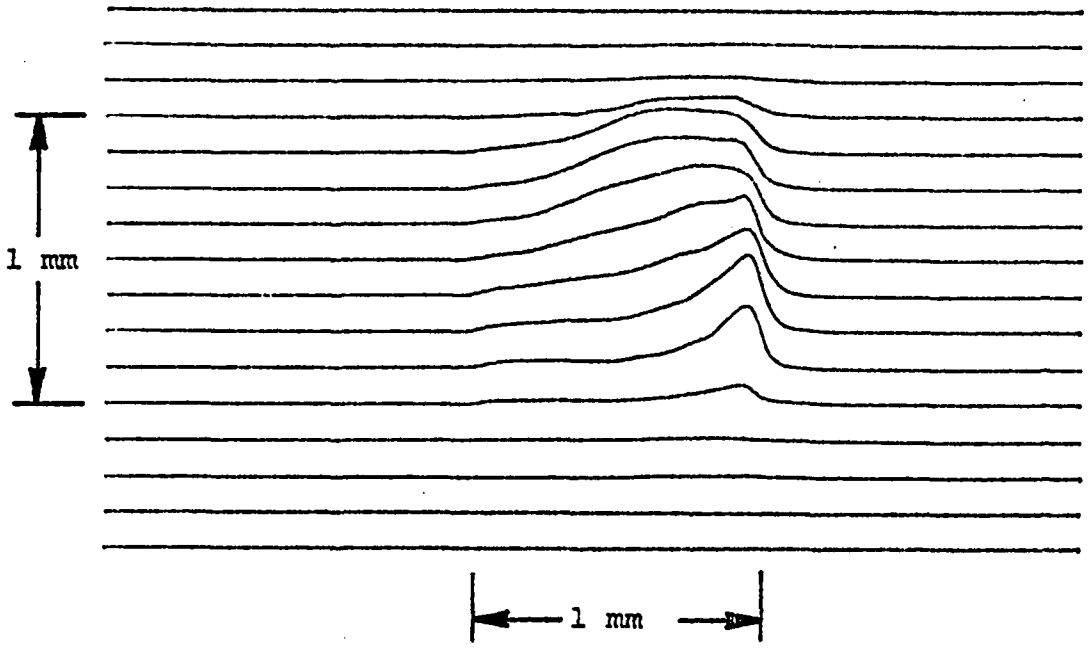

Fig. 7 Raster scan of another HgCdTe detector at 11.1 μm with a 25 μm diameter pinhole. The detector is 1 mm square with its peak sensitivity near 11 μm.

Figure 8 is a raster scan of one element in a quadrantal PbSnTe high speed detector. From visual inspection, this detector appears to be a mesa junction device approximately 125 μm square with an electrical lead attached at the center. The test wavelength was again 11.1 μm with a 25 μm pinhole diameter. The dimensions of this spatial sensitivity pattern again indicate a spot size of about 100 μm diameter.

The spatial maps in Figures 5-8 clearly demonstrate the variation in spatial sensitivity from one detector to the next. The detectors in Figures 6 and 7 have consecutive serial numbers and nearly identical manufacturer specifications. However there is a dramatic difference in their spatial uniformity. Also, the map of the PbSnTe element clearly and correctly displays the shadow of the twin electrical leads attached to the center of the detector.

3.3 Pulse Characteristics

Figure 9 is a recording of a detected optical pulse. For this test, the photovoltaic PbSnTe detector studied above was used without reverse bias or a preamplifier. Normally such pulse shapes would be photographed in real time on the oscilloscope supplied with the LS-2X; however, for this test a sampling oscilloscope with a risetime of 0.35 ns was used. The electrical pulse to the diode was supplied by the LCP whose essential components are a high voltage power supply, a mercury wetted reed pulser and a coaxial charge line. The length of the pulse and its falltime is determined by the length of the charge line.

The optical pulse in Figure 9 is 97.4 ns wide measured at the 50% points. The risetime, $t^r_{.1-.9}$, is 7.5 ns while the falltime, $t^f_{.1-.9}$, is 11.0 ns. The rise-and falltimes of the electrical input pulse were 0.46 ns and 3.6 ns respectively; the risetime measurement includes the 0.35 ns oscilloscope risetime. The differences between the observed optical pulse and the electrical pulse are due entirely to the detector and are an indication of the non-reverse biased response time of the detector.

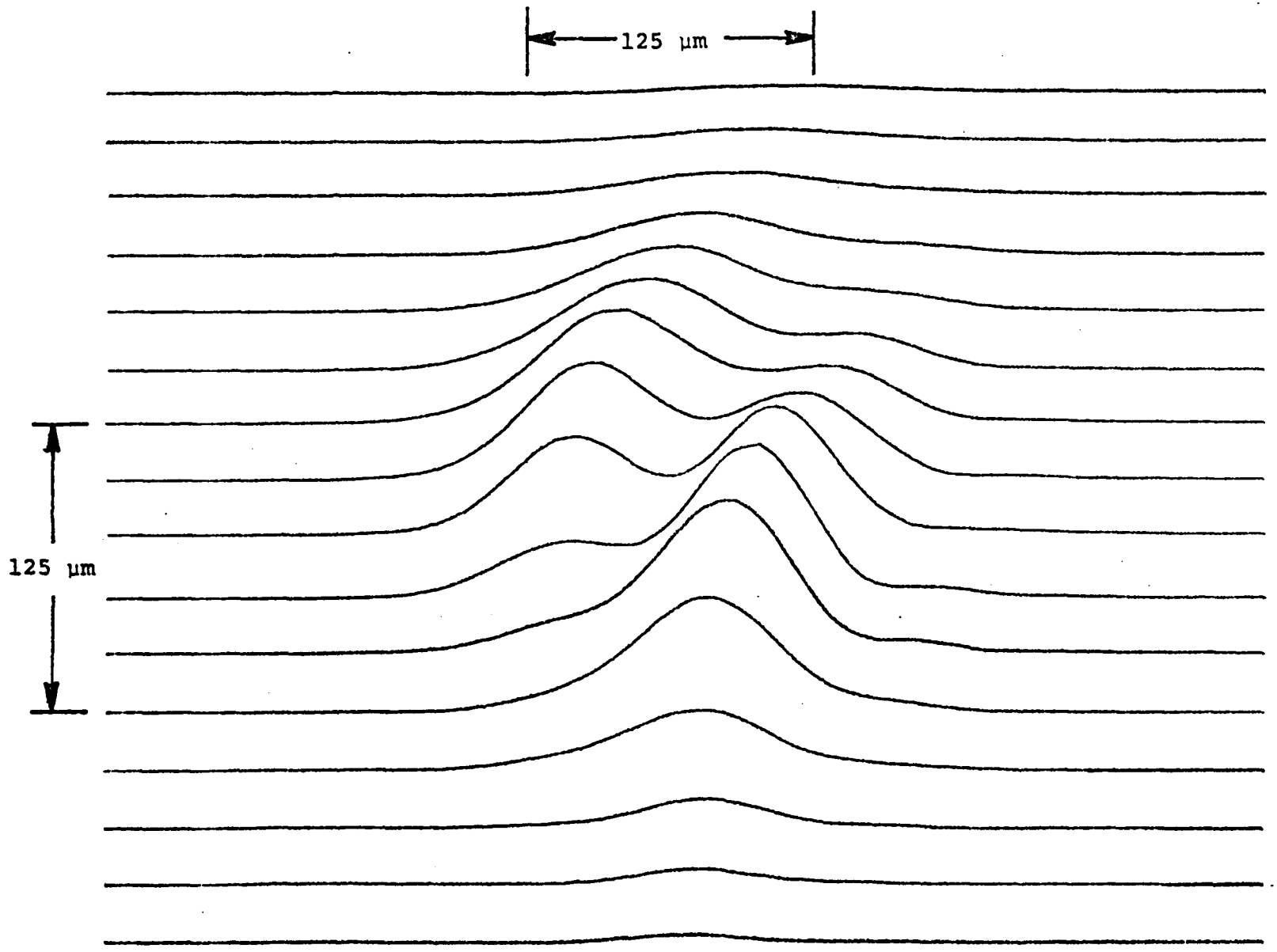

Fig. 8 Spatial sensitivity map of a pv PbSnTe mesa detector. The element size is approximately 125 µm square with an electrical lead in the center. The test wavelength was 11.1 µm.

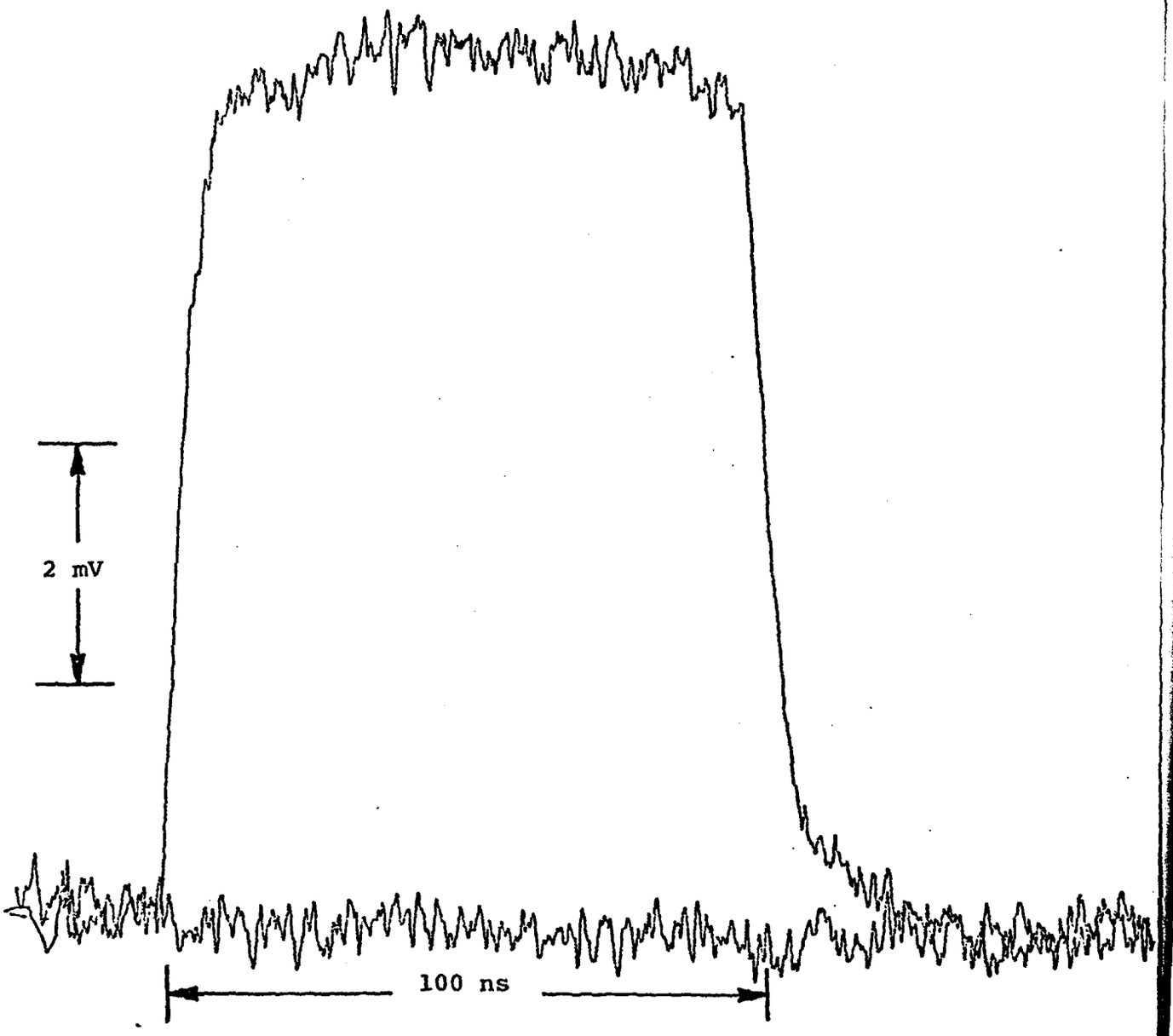

FIGURE 9

The upper trace is a 97.4 ns wide optical pulse. The lower retrace is with the laser beam blocked. The detector was a pv PbSnTe operated without bias current or a preamplifier. Risetime, $t^{r}_{.1-.9}$ = 7.5 ns, Falltime $t^{f}_{.1-.9}$ = 11.0 ns.

The actual rise and falltime of the optical pulse is much closer to that of the electrical pulse. This was confirmed in preliminary tests using a very high speed HgCdTe detector borrowed from Spears* and by independent unpublished measurements made by Nill and Spears.[6]

The falltime of the electrical pulse and hence the optical pulse is a function of the charge line length and hence will decrease with pulse width. For the 10 ns wide pulse the measured electrical falltime is less than 0.75 ns.

4.0 CONCLUSION

The original design criteria for the LS-2X Detector Test System contained three fundamental optical requirements

1) an output beam with spatial uniformity better than ± 10% over a 10 mm diameter circle;
2) a focused spot size of less than 100 μm at a wavelength of 5 μm;
3) pulsed operation with optical pulses of 10 ns and 100 ns widths and rise- and falltimes less than 5 ns.

All three fundamental requirements have been achieved. The far field diffraction pattern of the spatial filter provides beam uniformities of better than ± 10% over a 10 mm disc. Uniformities between ±5% and ±8% were observed.

In the focused spot option, several spatial profiles of different detectors were recorded in the 11 μm and 12.3 μm regions. All measurements indicate a spot size of about 100 μm in agreement with diffraction theory. Hence, the spot size, will definately be smaller than 100 μm at λ =5 μm.

Finally, 10 ns and 100 ns wide pulses with risetimes of less than 0.50 ns and falltimes of less than 4 ns were achieved.

* We wish to thank Dr. Spears of the MIT Laboratory for the use of his detector.

The LS-2X Detector Test System has the capability of performing detector array uniformity tests, spatial sensitivity mapping of single elements, and temporal response measurements, all at user specified wavelengths between 2.8 μm and 30 μm. The system capability can be easily expanded to include spatial mapping of the temporal response through the addition of a sampling oscilloscope plug-in. This addition is recommended since it also permits x-y recording of the temporal response function.

5.0 REFERENCES

1. D.L. Spears, Solid State Research MIT Lincoln Labs., No.3 p. 5, 1976.

2. C.Venkatesh, and A.W Mantz, private communication, 1979.

3. M.Born and E.Wolf, Principles of Optics, (Pergamon Press, Oxford, 1975), 392-398.

4. P.H. van Cittert, Z. Phys. 65, 547 (1930)

5. G.H. Godfrey, Aust. J. Sci. Res. 1, 1 (1948).

6. K.W. Nill and D.L. Spears, private communication, 1978.

6.0 APPENDIX

6.1 Operators Manual LS-2X Laser Source Detector Test System.